CHIRAL Rh/SiO₂ CATALYSTS FOR ENANTIOSELECTIVE HYDROGENATION REACTIONS. THE ROLE OF (S,S)-DIPAMP AS CHIRAL MODIFIER AND STABILIZER ON METALLIC NANOPARTICLES SYNTHESIS

CLAUDIO MELLA[1], MAURICIO ÁVILA[1], ARIEL SÁNCHEZ[1], TERESITA MARZIALETTI[2], PATRICIO REYES[1] AND DORIS RUIZ[1]*.

[1]*Universidad de Concepción, Facultad Ciencias Químicas, Edmundo Larenas 129, Concepción, Chile. Phone: (+056)41 2204324, Fax: (+056)41 2245974.*
[2] *Universidad de Concepción, Departamento Ingeniería Química, Barrio Universitario S/N. Concepción, Chile*

ABSTRACT

Rhodium nanoparticles were successfully stabilized by the *(S,S)*-1,2-ethanediylbis[(2-ethoxyphenyl)phenylphosphine] (*(S,S)*-DIPAMP) deposited on SiO₂ prepared by a facile reduction and impregnation method. The chiral catalysts obtained were efficient for the enantioselective hydrogenation reactions of prochiral compounds. The catalysts synthesized from [Rh(µ-OMe)(COD)]₂ in the presence of different amounts of a ligand used as chiral stabilizer, showed good metal dispersion. As shown by TEM, the metal particle size ranged between 1 and 2 nm using stabilizer and 9.1 nm was achieved without chiral ligand. Other techniques were used to characterize the chiral catalysts such as X-ray diffraction (XRD), electron diffraction, thermogravimetric analysis (TGA) and N₂ adsorption-desorption isotherms.

(S,S)-DIPAMP was used as the stabilizer of metal particles to prevent growing and agglomeration, and it also acts as chiral modifier inducing enantioselectivity in the asymmetric hydrogenation of 3,4-hexanodione (HD), ethyl pyruvate (EP), ketopantolactone (KP), and acetophenone (AP). Under specific conditions such as 25 °C, 40 bar of H₂ and substrate/Rh=100, 1%Rh-*(S,S)*-DIPAMP/SiO₂ chiral catalysts showed excellent catalytic performance with conversion and enantiomeric excess (ee) levels up to 99% and 54% respectively.

Keywords: *(S,S)*-DIPAMP, stabilized nanoparticles, enantioselective hydrogenation, rhodium, chiral ligand.

INTRODUCTION

Nowadays, catalysis is one of the most essential research areas of metal nanoparticles[1-3]. Controlled sized metal nanoparticles (NPs) have received considerable attention due to their high surface area compared to bulk catalytic materials[4-5]. Metal agglomeration is an undesired process, mainly in catalytic reactions, because it leads to loss some properties associated with the "nano state". Chiral stabilizer agents control metal growing generating high amount of metal particles on the asymmetry surface[6-13]. One of the strategies to take advantage of the abilities of the stabilizer agents and use them for catalytic applications is the deposition of chiral nanostructured metal colloids on catalyst supports such as SiO₂ and other mesoporous materials. Chiral modification of metal surfaces has expanding successfully the powerful potential of heterogeneous metal catalysts[14-15]. One of the most successful reactions in this area is the asymmetric hydrogenation of α, β-keto esters and ketones[16]. Synthesis of enantipure alcohols is of vital importance in pharmaceutical and flavoring industries[17-18]. Alcohols are commonly synthesized by metal NPs such as Rh, Ru, Ir and Pt. A few research groups have focused their studies in using chiral nanoparticles as catalysts. NPs have been also used as catalysts in reactions such as hydroformylation, allylic alkylation, hydrosilylations, Suzuki and Heck-type, couplings, among others achieving good results[19-26].

Considering previous statements, both composition of NPs and prevention of particle aggregation of immobilized systems are critical features required by heterogeneous catalysts to be used in enantiomeric reactions.

This paper report the effective performance of a synthesized catalysts having rhodium nanoparticles supported on SiO₂[14,15,27].

The catalysts were synthesized by reducing an olefin and ligand displacement from organometallic precursor in the presence of *(S,S)*-DIPAMP (see Fig. **1**) and SiO₂ on H₂. Adding different amounts of a chiral ligand controls the metal average diameters, increasing specific metal surface area, metal dispersion and also obtaining asymmetric heterogeneous catalysts useful in enantioselective hydrogenation of HD, EP, KP and AP, as shown in figure **1**. All products of these reactions have applications in chiral drugs syntheses[28-35].

EXPERIMENTAL

Unless noted otherwise, all experiments were carried out using standard Schlenk and vacuum-lines. Substrates and solvents used in this study were analytical grade and treated by standard methods[1,23,24].

Materials

RhCl₃·3H₂O, ethyl pyruvate (98%, 1.045 g mL⁻¹), cis,cis-1,5-cyclooctadiene (COD) ≥95%, *(S,S)*-DIPAMP (≥95%) and KOH (≥85%) were used as received from Aldrich without further purification.
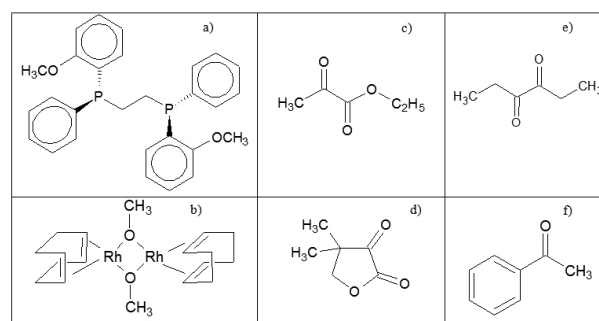

Figure 1. Chemical structure of a) *(S,S)*-1,2-ethanediylbis[(2-ethoxyphenyl) phenylphosphine] ligand, b) di-µ-methoxybis(1,5-cyclooctadiene) dirhodium as precursor, and c) ethyl pyruvate, d) ketopantolactone, e) 3,4-hexanodione and f) acetophenone as prochiral substrates.

Acetophenone (99.0%, 1.03 g mL⁻¹), was purchased from Fluka and distilled prior reactions.

Ketopantolactone (97%), 3,4-hexanodione (95%, 0.939 g mL⁻¹), pentane, tetrahydrofuran and dichloromethane (all of them from Aldrich), chloroform, cyclohexane, methanol, diethylether and ethanol (96%), all from Merck, were distilled prior reactions. THF was treated by metallic sodium. Precursors and catalysts were prepared under purified N₂ atmosphere.

N₂ and H₂ (99.995% of purity) were purchased from Linde. SiO₂ BASF was heated at 150 °C for 2 h before use to remove surface residues.

Chemical structure of keys compounds used in this work, such as the chiral ligand, organometallic precursor and substrates are shown in Figure **1**.

Synthesis of organometallic precursor

The organometallic precursor [Rh(µ-OMe)(COD)]₂ was prepared from Rh(µ-Cl)(COD)]₂.

Rh(µ-Cl)(COD)]₂ was synthesized from RhCl₃·3H₂O (0.5 g, 2.0 mmol) and 1.1 mL of COD in 20 mL of ethanol were stirred under reflux at 70 °C for 3 hours obtaining a yellow precipitate (*eq. 1*). It was filtered and washed with cold diethyl ether at 5 ºC collecting 71% of total solid. The following reaction is taking place during preparation.

$$2RhCl_3 + 2COD + 2CH_3CH_2OH \rightarrow [Rh(\mu\text{-}Cl)(COD)]_2 + 4HCl + 2CH_3CHO \ (eq. \ 1)$$
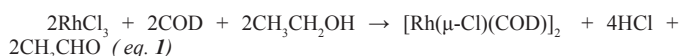
Finally, [Rh(µ-Cl)(COD)]₂ (175 mg, 0.36 mmol) dissolved in

dichloromethane (15 mL) was added to a solution of KOH (40 mg, 0.71 mmol) in methanol (5 mL). Immediately a dark yellow solid, $[Rh(\mu\text{-OMe})(COD)]_2$ see *eq. 2*, precipitates. After 30 minutes of stirring at room temperature, the solvent was removed under vacuum. Yellow precipitate was mixed with 10 mL of methanol and 15 mL of water. Then, the solution was filtered, washed (H_2O, 3x5 mL) and finally under dried vacuum without further purification. The yield of this step was 75%. The reaction controlling this step is represented below:

$$[Rh(\mu\text{-Cl})(COD)]_2 + 2KOH + 2MeOH \rightarrow [Rh(\mu\text{-OMe})(COD)]_2 + 2KCl + 2H_2O \quad (eq.\ 2)$$
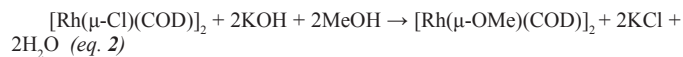
Synthesis of metal NPs supported

The precursor, $[Rh(\mu\text{-OMe})(COD)]_2$ was dissolved in 80 mL of THF, in the presence of certain amount of *(S,S)*-DIPAMP ligand (L). The Rh/L ratio varied from 0.2 to 1.0. The metal was reduced at 25 °C and 3 bar H_2 under stirring for 20 h.

Appropriate amount of rhodium nanoparticles was added onto dried SiO_2 obtaining 1wt% of Rh NPs on SiO_2. THF was added at the mixture, it was stirred overnight at 298 K, and then it was dried under vacuum for 3 h. Finally, chirally modified catalyst was washed overnight with pentane (3 x 25 mL) under vacuum at 40 °C.

Rhodium nanoparticles and 1wt% supported rhodium nanoparticles samples were labeled as **Rh-xL** and **Rh-xL/Si,** respectively, were **L** represents *(S,S)*-DIPAMP and **x** represents molar ratio of rhodium to ligand (Rh/L) ratio.

Catalysts characterization

Metal particle size (diameter) was determined by transmission electron microscopy (TEM) and electron diffraction using JEOL JEM-1200 model EXII. Metal dispersion on SiO_2 was calculated from the relationship between surface and total atoms. Additionally, mean particle size (cubic model) was also estimated by TEM.

Nitrogen adsorption-desorption isotherms at 77 K were obtained in a Micromeritics ASAP 2010 (CHEMI). Brunauer, Emmett and Teller (B.E.T) and Barrett, Joyner and Halenda (B.J.H) models allowed to obtain specific surface area, pore diameter and pore volume of all catalysts tested in this study.

XRD analyzes were performed using Rigatu New X-Ray "Geigerflex" D/max-IIC (40 Kv, 2 mA) diffractometer in the 2θ range of 10 ° to 90 ° (λ=1.54056 Aº) at 1 °/min. XRD allows to identify the phases present in the catalysts.

TG analyses were conducted by TGA/SDTA 851ᵉ Mettler Toledo Thermogravimetric Analyser on 100 mL/min Helium from 30 ºC to 800 ºC at 10 ºC/min. TG technique allows to relate the mass loss versus temperature and possible interactions between metal and ligand.

Enantioselective hydrogenations reactions

Hydrogenation reactions were performed in a stainless steel semibatch reactor coated with Teflon. Typically, 50 mL of solvent was used in all reactions at 40 bar of pressure, room temperature, stirring speed of 800 rpm, and molar ratio [substrate/metal] of 100. The solvent used for HD, EP and AP substrates was cyclohexane and toluene for KP.

The experimental conditions used in this study were carefully selected to avoid mass transfer limitations.

Analyses of reagents and products concentrations were determined using a SHIMADZU GC-MS, model QP5050, equipped with a chiral column Beta DEX 225 (Supelco) of 30 m long and 0.25 mm of diameter. Carrier gas used was helium (99.995% of purity). Optical yields expressed as ee values, were calculated with the following equation:

$$ee\ (\%) = ([R]-[S])/([R]+[S]) \times 100 \quad (eq.3)$$

ee_{max} indicates the highest enantioselectivity value reached at the end of selected reaction, when reactant conversion was completed.

RESULTS AND DISCUSSION

Catalysts characterization

Stabilized Rh nanoparticles showed smaller metal diameters than non-stabilized Rh NPs for both free and supported NPs. Accordingly, stabilized rhodium NPs exhibited high dispersion (58%) having average metal diameter lower than 2 nm (see table **1**). Conversely, non-stabilized Rh NPs displays an average metal diameter as high as 9.1 nm showing metal dispersion of 10%. Additionally, results showed in table **1** revealed that stabilized free and stabilized supported Rh nanoparticles posses similar metal particle size. Figure **2** shows particle size distribution and TEM micrographs and of Rh

samples. As expected, these observations connected stabilizing properties of the *(S,S)*-DIPAMP ligand with the control of the agglomeration of supported nanoparticles, making this procedure a useful, easy and reproducible method of preparing materials for catalytic purposes[1,13,15].

Table 1. Average particle size (d) and metal dispersion (D) of free, stabilized and supported NPs.

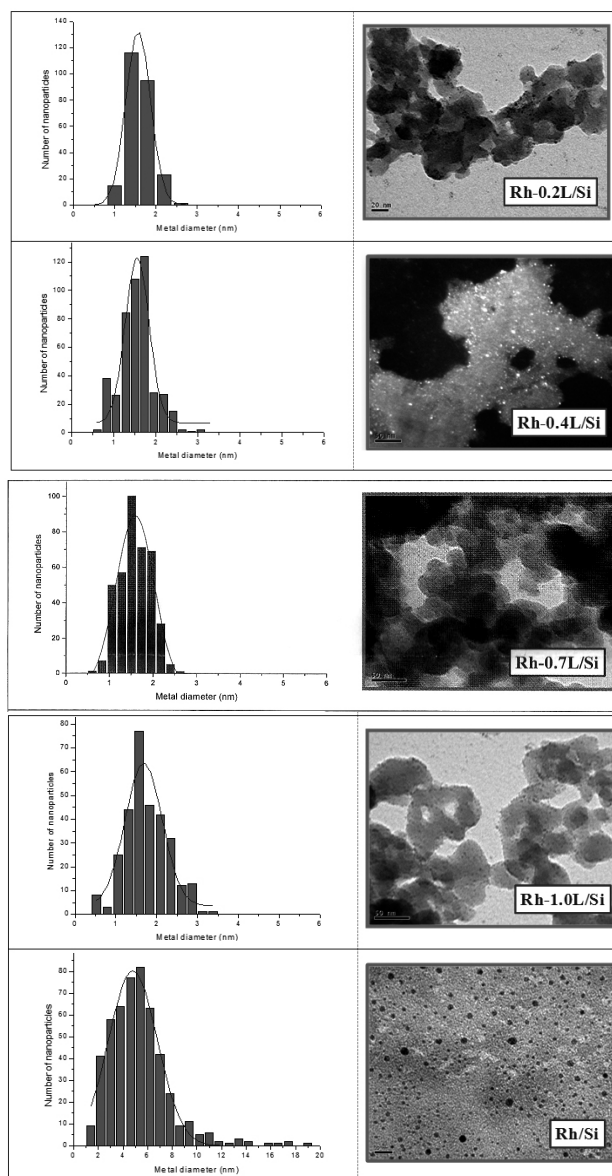| Sample	d_{TEM} (nm)	D (%)
Rh	4.8	-
Rh/Si	9.1	10
Rh-0.2L	1.5	-
Rh-0.2L/Si	1.6	58
Rh-0.4L	1.5	58
Rh-0.4L/Si	1.6	
Rh-0.7L	1.5	-
Rh-0.7L/Si	1.6	58
Rh-1.0L	1.5	-
Rh-1.0L/Si	1.7	54

Figure 2. Size distribution histograms and TEM micrographs and of stabilized and non-stabilized Rh catalysts.

Specific surface area and pore volume determined from N_2 adsorption-desorption isotherms are displayed in Table **2**. Supported samples, in agreement to the classification Brunauer, Deming, Deming and Teller (B.D.D.T), showed type IV isotherms with a hysteresis loop. The isotherms are characteristic of mesoporous solids mainly with pores cylindrical geometry. Specific surface area values ranged from 136 to 76 (m² g⁻¹) for non-stabilized Rh and stabilized catalysts, respectively indicating that ligand partially blochs the propus structure of the support. The average pore diameter decreased from 31 to 18 nm as stabilized nanoparticles were deposited onto the pores of the support. The molecular diameters of prochiral substrates are considerably smaller than the pore diameter of the material. Therefore, it allows an appropriate diffusion of the reactants and products from to the active sites.

Table **2** also compiles results obtained from TG analyses. All supported catalysts show thermograms indicating that desorption of physisorbed water is completed at 150°C and is followed by a broad region of weight loss, due to dehydroxylation process. In thermograms the maximum loss of mass is above to 400 °C until 550 °C. It can be seen an important increase of % weight loss according with the amount of *(S,S)*-DIPAMP added in the NPs synthesis, indicative of the chiral ligand is on catalysts surface. Decomposition around 500 °C is indicating that there is likely a chemical interaction between *(S,S)*-DIPAMP and Rh/SiO₂, as shown previous reports[36].

Table 2. Surface area, pore volume and mass loss of stabilized and non-stabilized Rh catalysts.

Catalyst	$S_{B.E.T}$, m² g⁻¹	V_{pore}, cm³ g⁻¹	% wt loss[a]
Rh/Si	136	31	7.0
Rh-0.2L/Si	84	19	7.8
Rh-0.4L/Si	80	18	8.4
Rh-0.7L/Si	76	18	8.7
Rh-1.0L/Si	81	19	8.9

[a] % wt loss from 350 °C up to 600 °C.

No visible diffraction lines attributable to rhodium crystalline phase of Rh-(x)L/Si catalysts appeared in XRD patterns, due to Rh has small particle diameter and the metal loading in these catalysts were was 1% wt of rhodium. On the contrary, non-stabilized Rh catalyst diffraction peaks, which had higher average particle diameter, showed up $2\theta = 41.0°$ and 47.3° representing (111) and (200) planes of rhodium phase[37]. The most intense peak at 41.0 ° was corroborated by electron diffraction analysis showing Rh (111). As mentioned elsewhere, XRD and electron diffraction analysis allow to verify crystalline components on solid catalysts. Finally, electronic state of Rh on the surface of each catalyst, after exposure to H_2 at 30 °C for 1 h, was analyzed by XPS showing that rhodium-phase was mainly reduced. Previous work confirmed that rhodium $3d_{5/2}$ appears mainly reduced at 307.3 eV binding energy[14,15].

Enantioselective hydrogenation reactions

The main objective of this study was to investigate catalytic activity and selectivity in enantioselective hydrogenation reactions of supported rhodium NPs stabilized by *(S,S)*-DIPAMP. Additionally, the nature of the substrate and (S,S)-DIPAMP loading on supported rhodium NPs were also studied.

Typically, asymmetric hydrogenation of EP (Fig. **3**a) is used as test reaction in order to evaluate both activity and enantioselectivity of new catalysts[16]. Consequently, Rh-xL/SiO₂ catalysts were tested on the enantioselective hydrogenation of EP, showed in Figure **3**b, exhibiting good performance in the transformation of EP.

According to previous works, as expected, the addition of a phosphorous ligand such as *(S,S)*-DIPAMP allows to obtain the preferential formation of the *(R)* with respect to *(S)* isomer[15]. In Figure **3**c is shown the preferential formation of *(R)*-ethyl lactate using Rh-0.4L/Si catalyst.
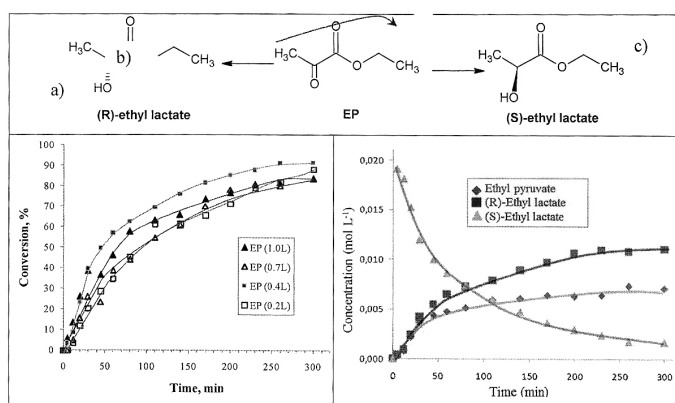

Figure 3. Enantioselective hydrogenation of EP a) Reaction scheme, b) conversion of EP on time with Rh-xL/Si catalysts and c) evolution of the hydrogenation of EP on time using **Rh-0.4L/Si**. Reaction conditions: 0.02 mol L⁻¹, at 40 bar of H_2, 298 K and cyclohexane as solvent using 100 mg of catalysts.

The formation of 4-*(R)*-hydroxy-3-hexanone from HD achieved values up to 54%. Maximum conversion was 94% at 300 min (Table **3**, Fig. **4**). Although, similar behavior was expected for the reaction of AP, an aromatic ketone, low conversion was observed due probably to an increased interaction of the aromatic ring with the surface of the catalysts. However, further studies are needed to draw a conclusion. This work shows promising results of enantioselectivity in very scarcely studied substrates to date[14,15].
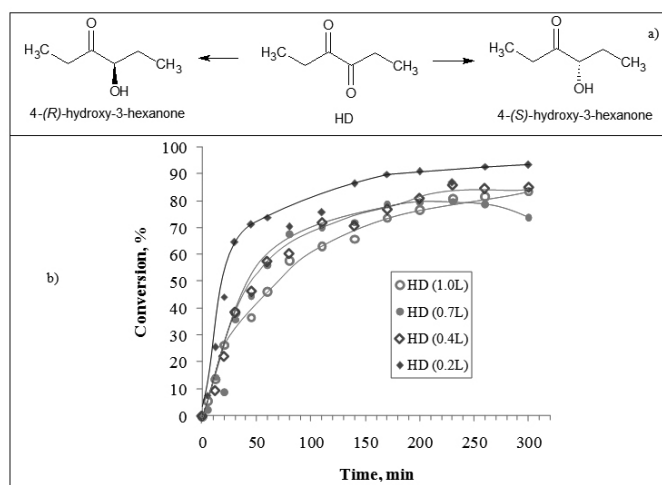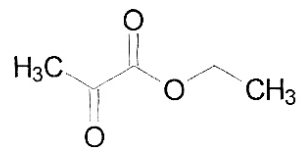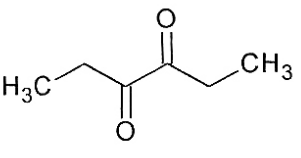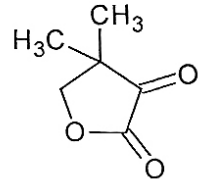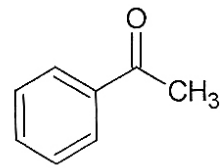

Figure 4. Enantioselective hydrogenation of HD, under following reaction conditions: 0.02 mol L⁻¹, 100 mg of Rh-xL/Si catalysts in cyclohexane at 40 bar of H_2 and 298 K. a) Reaction scheme, b) conversion on time.

The activity of Rh-xL/Si catalysts in the enantioselective hydrogenation of KP is showed in Figure **5**. All catalysts achieved complete conversion of KP excepting Rh-0.4L/Si. Among all reactants tested, KP was quickly converted at low reaction time attributed to high reactivity of these ketones. Furthermore, keto group reactivity increases with the presence of the ester carbonyl group in α position[38].

In contrast to high conversion of KP, low ee values were accomplished as shown in Table **3**. This low enantioselectivity is probably because KP preferred unmodified metal sites. The induction time observed on Rh-0.4L/Si catalyst may be due to formation of dimers of KP. These side reactions may be limiting enantiodifferentiation.

Contamination of catalyst surfaces can not be argued as a reason of the induction time observed in this system, because it is well known that clean surfaces are favored when organometallic precursors were used in the preparation of heterogeneous catalysts[29].

Table 3. Conversion, enantioselectivity values and pseudo first-order rate constants of hydrogenation reactions of HD, EP, AP and KP. Conditions: 0.02 mol L^{-1} of substrate and 100 mg of Rh-xL/Si catalysts in cyclohexane at 298 K and 40 bar of H_2.

Substrate	Catalyst	% Conv.[a]	k (min^{-1} g$_{cat}^{-1}$ mol 10^{-4})[b]	% ee$_{max}$[c]
EP	Rh 0.2-L/Si	49	0.17	19
	Rh 0.4-L/Si	91	0.63	26
	Rh 0.7-L/Si	84	0.32	13
	Rh 1.0-L/Si	84	0.48	7
HD	Rh 0.2-L/Si	94	1.12	41
	Rh 0.4-L/Si	85	0.62	23
	Rh 0.7-L/Si	74	0.59	47
	Rh 1.0-L/Si	85	0.52	54
KP	Rh 0.2-L/Si	98	0.92	8
	Rh 0.4-L/Si	77	0.12	19
	Rh 0.7-L/Si	100	1.01	12
	Rh 1.0-L/Si	100	0.92	8
AP	Rh 0.2-L/Si	83	0.73	11
	Rh 0.4-L/Si	36	0.11	46
	Rh 0.7-L/Si	78	0.09	15
	Rh 1.0-L/Si	70	0.01	14

[a]% Conversion at 300 min of reaction. [b] Pseudo first-order rate constants was calculated up to 60 min. [c]% ee max referred to maximum value of *(R)*-enantiomer.
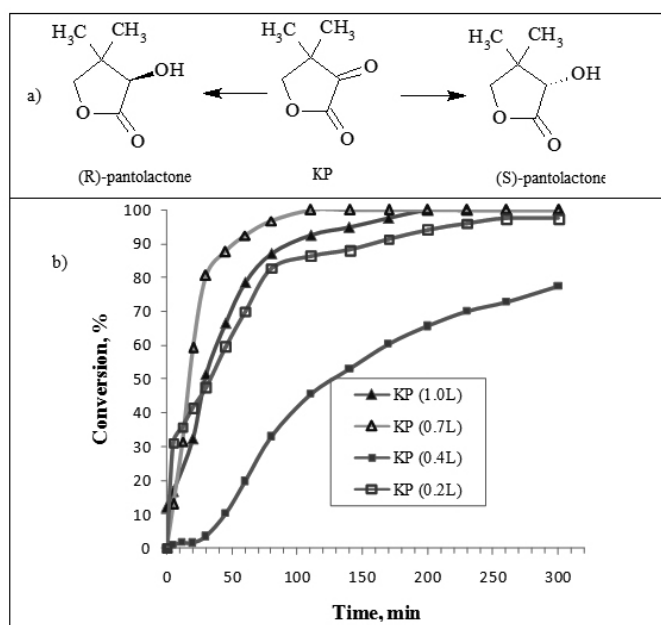
Figure 5. Enantioselective hydrogenation of KP. a) Reaction scheme, b) conversion on time under reaction conditions: 0.02 mol L^{-1}, 100 mg of Rh-xL/Si catalysts, 40 bar of H$_2$ and 298 K in cyclohexane as solvent.

Evolution of the enantioselective conversion of AP up to 300 minutes is shown in Figure **6**, and maximum enantioselectivity and maximum conversion values are compiled in Table **3**. It was found that Rh 0.2-L/Si achieved maximum values of conversion (83%) among all catalysts tested in this system, but lowest enantioselectivity value (46%). In contrast, Rh 0.4-L/Si achieved highest value of enantioselectivity in this system (46%), but lowest value of conversion (36%).
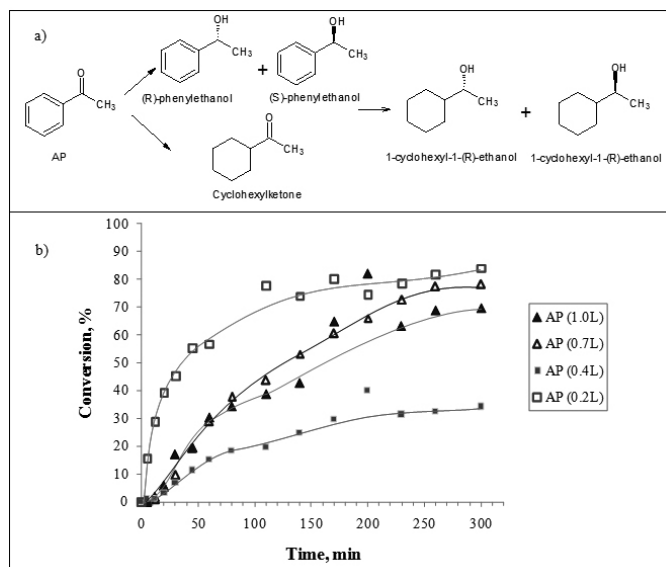

Figure 6. AP hydrogenation: a) reaction scheme, b) evolution of conversion on time. Reaction conditions: 0.02 mol L^{-1} of AP, 100 mg of Rh-xL/Si catalysts, 40 bar of H$_2$ and 298 K in cyclohexane as solvent.

Finally, stability and reproducibility of this preparation method were also considered in this study. Accordingly, preliminary studies using Rh/SiO$_2$ catalysts indicated that conversion values of EP can be keep for at least 3 cycles. Additionally, previous results also suggested no leaching of Rh during reaction.

CONCLUSIONS

Chiral NPs can be synthesized under mild conditions using *(S,S)*-DIPAMP as metal particle stabilizer. Stabilized supported Rh nanoparticles show metal average smaller than 2.5 nm, with 58% of dispersion showing that aglomeration of NPs can be controlled by this preparation method. Consequently, it was shown that asymmetric catalysts tested for this study showed both high activity and enantiomeric resolution in the evaluated reactions. Rh-0.2L/Si catalyst was the most active catalyst for HD and AP enantioselective reactions, whereas for the hydrogenation of KP was the Rh-0.7L/Si catalyst. Ethyl pyruvate showed lower activity and selectivity levels with these catalysts. In the hydrogenation of HD and AP, 54% and 46% of enantiomeric excess were obtained, respectively. It was also found that ketones hydrogenation led to higher ee than α-keto esters hydrogenations reactions. This paper shows that the activity and selectivity of catalysts are directly related to the size and nature of the metal nanoparticles. Non stabilized catalysts generated wide distribution of metal sizes on solids and makes impossible the repeatability in hydrogenation reactions, obtaining racemic mixtures of products.

REFERENCES

1. A. Roucoux, J. Schulz, H. Patin, *Chem. Rev*. **102**, 3757, (2002).
2. H. Bönnemann, G. A. Braun, *J. Chem. Eur.* **3**, 1200, (1997).
3. H. Bönnemann, G. A. Braun, *Angew. Chem. Int. Ed*. **35**, 1992, (1996).
4. B. Chaudret, *C. R. Physique*. **6**, 117, (2005).
5. H. Bönnemann, R. M. Richards, *Eur. J. Inorg. Chem*. **10**, 2455, (2001).
6. P. Barbaro, V. Dal Santo, F. Liguoric, *Dalton Trans*. **39**, 8391, (2010).
7. D. Han, X. Li, H. Zhang, Z. Liu, J. Li, C. Li, *J. Catal.* **243**, 318, (2006).
8. D. Han, X. Li b, H. Zhang, Z. Liu, G. Hu, Can Li, *J. Mol. Cat A: Chem*. **283**, 15, (2008).
9. W. Xiong, H. Ma, Y. Hong, H. Chena, X. Lia, *Tetrahedron Asym*. **16**, 1449, (2005).
10. M. Jacinto, P. Kiyohara, S. Masunaga, R. Jardim, L. Rossi, *Appl. Catal. A: General*. **338**, 52, (2008).
11. R. Somanathan, N. Cortez, M. Parra-Hake, D. Chávez, G. Aguirre. *Mini-Rev. Org. Chem***, 313**, 5, (2008).
12. S. Nath, S. Jana, M. Pradhan, T. Pal, *J. Colloid Interface Sci,* **341**, 333 (2010).
13. A. Roucoux*, Top*. *Organomet. Chem*. **16**, 261, (2005).
14. D. Ruiz, C. Mella, J. L. García Fierro, P. Reyes, *J. Chil. Chem. Soc.* **57**, 1199, (2012).
15. D. Ruiz, M. Oportus, C. Godard, C. Claver, J.L García Fierro, P. Reyes, *Curr. Org. Chem*. **16**, 2754, (2012).
16. Y. Orito, S. Imai, S. Niwa, *J. Chem. Soc. Jpn*. **92**, 1118, (1979).
17. P. Subramanian, S. Chatterjee, M. Bhatia, *J. Chem.Technol. Biotechnol.* **39**, 215, (1987).
18. D. Gala, D. DiBenedetto, J. Clark, B. Murphy, D. Schumacher, *Tetrahedron Lett.* **37**, 611, (1996).
19. T. Marzialetti, J.L.G. Fierro, P. Reyes, *J. Chil. Chem. Soc.* **50**, 391, (2005).
20. D. Ruiz, J.L.G. Fierro, P. Reyes. *J. Braz. Chem. Soc.* **21**, 262, (2010).
21. A. Gual, C. Godard, K. Philippot, B. Chaudret, A. Denicourt-Nowicki, A. Roucoux, S. Castillón, C. Claver, *Chem. Sus. Chem.* **2**, 769, (2009).
22. T. Marzialetti , M .Oportus, D. Ruiz, J. L. García Fierro, P. Reyes, *Catal. Today*. **133**, 711, (2008).
23. A. Gual, M. R. Axet, K. Philippot, B. Chaudret, A. Denicourt-Nowicki, A. Roucoux, S. Castillón, C. Claver, *Chem. Commun*. 2759, (2008).
24. S. Castillon, C. Claver, Y. Diaz, *Chem. Soc. Rev*. **34**, 702, (2005).
25. M. Studer, H. U. Blaser, C. Exner, *Adv. Synth. Catal*. **345**, 45, (2003).
26. J. Dupont, G. S. Fonseca, A. P. Umpierre, P. F. P. Fichtner, S. R. Teixeira, *J. Am. Chem. Soc.* **124**, 4228, (2002).
27. D. Ruiz, P. Reyes, *J. Chil. Chem. Soc*. **53**, 1740, (2008).
28. P. Ellaiah, K. Krishna, *Indian Drugs*. **24**, 192, (1987).
29. A. Roucoux, M. Devocelle, J. Carpentier, F. Agbossou, A. Mortreoux, *Synlett.* **4**, 358, (1995).
30. T. Morimoto, H. Takahashi, K. Achiwa, *Chem. Pharm. Bull*. **42**, 481, (1994).

31. M. Heitbaum, F. Glorius, I. Escher, *Angew. Chem. Int. Ed.***45**, 4732, (2006).

32. R. Schmid, *Chimia*. **50**, 110, (1996).

33. H. Brunner, A. Apfelbacher, M. Zabel, *J. Inorg. Chem.* **4**, 917, (2001).

34. T. Sturm, W. Weissensteiner, F. Spindler, K. Mereiter, A. Lopez-Agenjo, B. Manzano, F. Jalon, *Organometallics*, **21**, 1766, (2002).

35. J. Sonnenberg, N. Coombs, P. Dube, R. Morris, *J. Am. Chem. Soc*, **134**, 5893, (2012).

36. H. J. Zhu, Y. J. Ding, L. Yan, J. M. Xiong, Y. Lu, L. W. Lin, *Catal. Today*, **93**, 389, (2004).

37. J. Haglund, A. Guillermet, G. Grimvall, M. Korling, *Phys. Rev. B*, **48**, 11685, (1993).

38. X. B. Zuo, H. F. Liu, D. W. Guo, X. Z. Yang, *Tetrahedron*. **55**, 7787, (1999).